The Frequency Regulation Control Method of Large-Scale Distributed Energy Storage Systems in the Smart Grid

Yong Sun[1,*], Yuchen Hao[1], Xiao Li[1], Bo Ding[2], Hao Li[2], Jianwei Guan[3]
[1]State Grid Jiangsu Electric Power Co., Ltd.,
Nanjing, 210024, China
[2]State Grid Jiangsu Electric Power Co., Ltd., Huai'an Power Supply Branch,
Huai'an Jiangsu, 223001, China
[3]NARI Nanjing Control System Co., Ltd.,
Nanjing, 211106, China
[*]xzsy@163.com; hao_yuchen@126.com; jsdttyphoon@163.com; dingbo.ha@qq.com; 731718490@qq.com; guanjianwei@sgepri.sgcc.com.cn

***Abstract*—As the penetration rate of renewable energy in new power systems continues to increase, these systems face serious frequency control issues. The limitations of traditional methods for addressing frequency control lie primarily in their reliance on the frequency regulation capability of a single battery energy storage system (BESS). This dependence not only requires a complex communication infrastructure to transmit remote control signals but also is susceptible to communication delays, leading to system instability. This paper proposes a distributed BESS robust frequency control method (load frequency control (LFC)) based on a sparse communication network, aiming to address the limitations of traditional methods in terms of communication infrastructure requirements and the impact of communication delays. Subsequently, a dual-layer model predictive control (MPC) strategy is designed. The first layer uses a nominal model for predictive control, while the second layer considers system uncertainties for auxiliary control to improve the response characteristics of the BESS, thus significantly enhancing LFC performance and achieving more effective frequency regulation. Finally, simulation results show that under different parameter conditions, such as capacity, state of charge (SoC), and time constants, the response capability and frequency regulation effect of the distributed BESS are significantly better than those of traditional methods.**

***Index Terms*—Energy storage system; Load frequency control; Model predictive control.**

I. INTRODUCTION

As the proportion of traditional generators in power systems gradually decreases and the penetration rate of renewable energy sources (RES) continues to increase, the demand for load frequency control (LFC) in power systems is becoming increasingly urgent [1]–[3]. Moreover, the unpredictable and fluctuating nature of renewable energy sources makes it very difficult to control the frequency in power systems. The emergence of distributed battery energy storage systems (BESSs) offers an effective solution to address these issues [4], [5].

To date, substantial research progress has been made in the frequency regulation of power systems utilising distributed BESS. Researchers have integrated BESSs as an integral component of power systems to provide frequency control reserves in [6]. In [7], a method for controlling the state of charge (SoC) of batteries in a battery energy storage system for load-frequency control is proposed. The authors in [8] investigate the effect on the lifetime of the lithium-ion BESSs of various strategies to re-establishing the SoC of batteries after the primary frequency regulation. The authors in [9] examine the frequency control problem for power systems with multiple distributed BESSs, and a dual-consensus-based approach is presented for distributed frequency control. In [10], a distributed control strategy is proposed to coordinate multiple battery energy storage systems to support frequency regulation in power systems with a high penetration of renewable generation. In [11], a novel coordinated control algorithm is proposed for a distributed battery energy storage system and the neighbouring BESSs of a simulation system are grouped and controlled by a main control centre. The primary objective of the proposed coordinated control scheme is to mitigate voltage and frequency deviations. The authors in [12] consider a two-level profit-maximising strategy, including planning and control, for battery energy storage system (BESS) owners who participate in the primary frequency control market. The authors in [13] develop control strategies and provide guidelines for harmoniously operating a distributed multiple energy storage system for frequency regulation considering their respective SoC. In [14], a battery aggregator is considered that coordinates a number of distributed BESSs to provide primary frequency control service in the ancillary service market.

Given the limited frequency regulation capacity of individual BESS, aggregating a large number of BESS with varying characteristics for frequency regulation has emerged as a primary research focus. Compared to a single battery

Manuscript received 30 April, 2024; accepted 17 July, 2024.
This research was supported by the Science and Technology Project of State Grid Jiangsu Electric Power Company under Grant No. J2023117.

energy storage system, a BESS aggregator, which combines multiple BESS units, offers greater power and capacity, making it possible for system operators to control them as a single unified system. However, this methodology requires a comprehensive communication infrastructure to relay remote control signals from the control centre to the distributed BESS. The advent and progression of wide area monitoring systems (WAMS) facilitate the use of remote signals in wide area control (WAC) to achieve this objective [15], [16]. However, communication delays can significantly affect data measurement and control signals, reducing the effectiveness of frequency regulation and possibly causing system instability. Consequently, the impact of time delays must be carefully considered when designing BESS for frequency regulation. Model predictive control (MPC) is considered an effective solution in modern control systems and has become the preferred method to address these challenges [17]–[20]. Like in [17], the LFC state space model incorporating the dynamic model of wind turbines (WTs) is derived by combining the original dynamic models of the power system LFC with the dynamic models of wind turbines, then a predictive model is established and a novel MPC control strategy is proposed based on the predictive model and the formulation of the MPC optimisation problem.

Building on this, this paper introduces a multi-area load frequency control method for power systems incorporating distributed BESS, utilising a dual-layer MPC approach. The proposed methodology is adept at managing uncertainties in the operation of a power system. The inner layer uses a basic MPC that assumes that there are no uncertainties to predict the area control error (ACE) for a simple system. This control signal, along with its ACE, is combined with the ACE from the real system that has uncertainties, using the auxiliary MPC to create control signals for the BESS aggregator. To obtain the best control signal, optimisation steps are performed within the MPCs, considering the limitations of battery and system operations.

II. THE LPF MODEL BASED ON DUAL-LAYER MPCS

A. Frequency Control Architecture of Multi-Area Power Systems

Figure 1 shows a diagram illustrating the control scheme of distributed battery energy storage system (BESS) in a multi-region power system.

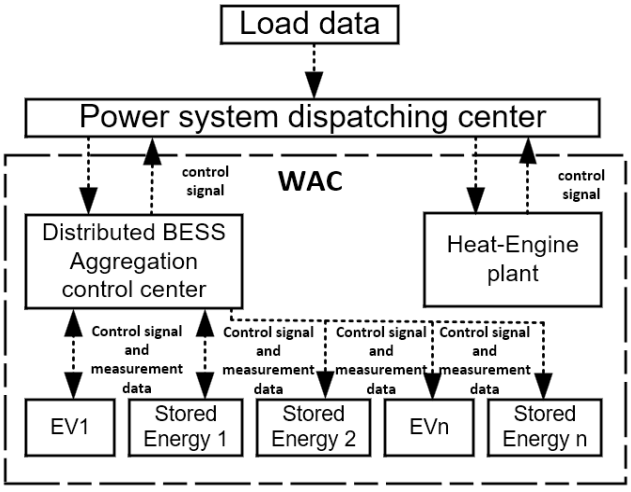

Fig. 1. Diagram of distributed BESS participating in LFC.

From Fig. 1, it is clear that a significant number of distributed BESS units are integrated into the power system through BESS aggregators. Different BESS units typically have varying capacities, charge/discharge efficiencies, and state of charge (SoC) levels. The distributed BESS aggregation control centre must establish a frequency control method for each BESS based on these characteristics. The power system dispatch centre sends frequency regulation requirements to the BESS aggregator control centre. The aggregator centre then sends the frequency adjustment amount and the duration of the area control error (ACE) to the BESS units involved, ultimately achieving frequency regulation of the power system. If the aggregator in region i manages $N_{B,i}$ distributed BESS units, the output power of the BESS aggregator is

$$\Delta P_{AG_i} = \sum_{b=1}^{N_{B,i}} \Delta P_{B_{i,b}}, \quad i \in M, \tag{1}$$

where $P_{B_{i,b}}$ represents the output power of the b^{th} BESS in region i and M represents the set of control areas. The control area is assumed to contain a thermal power plant, a wind farm, and a BESS aggregator. The frequency deviation of the control area can be expressed as [21]

$$\Delta \dot{f}_i = -\frac{D_i}{2H_i}\Delta f_i - \frac{1}{2H_i}\Big(\Delta P_{L_i} - \Delta P_{m_i} - \Delta P_{w_i} - \sum_{b=1}^{N_{B_i}} \Delta P_{B_{i,b}} + \Delta P_{tie_i}\Big). \tag{2}$$

In this equation, ΔP_{L_i} and ΔP_{m_i} represent the active power changes of the load and thermal power plant, respectively, H_i and D_i represent the inertia constant of the thermal power plant and the load damping coefficient, respectively, and ΔP_{tie_i} represents the total power change across the tie lines between region i and neighbouring regions

$$\Delta \dot{P}_{tie_i} = 2\pi \sum T_{ij}(\Delta f_i - \Delta f_j),\ j \in M - \{i\}, \tag{3}$$

where T_{ij} denotes the synchronisation torque coefficient of the tie line between regions i and j. If the wind turbine does not contribute to load frequency control, ΔP_{w_i} represents the change in output power of the wind turbine. The change in output power of BESS participating in frequency regulation can be expressed as

$$\Delta P_{B_{i,b}}(s) = \frac{K_{B_{i,b}}}{1+T_{B_{i,b}}s} U_{B_i}(s). \tag{4}$$

In this equation, $K_{B_{i,b}}$ and $T_{B_{i,b}}$ represent the charge and discharge coefficient and time constant of the BESS, respectively, and U_{B_i} denotes the control signal received from the BESS control centre. If communication time delays are ignored, it can be expressed as

$$\Delta P_{B_{i,b}} = \frac{-1}{T_{B_{i,b}}} \Delta P_{B_{i,b}} + \frac{K_{B_{i,b}}}{T_{B_{i,b}}} U_{B_i}. \tag{5}$$

The ACE is calculated as the sum of the power deviation across the tie lines and the weighted frequency deviation

$$ACE_i = \Delta P_{tie_i} + \beta_i \Delta f_i, \tag{6}$$

where β_i is the coefficient of the frequency deviation. The ACE signals provided to the thermal power plant and the BESS aggregator are as follows

$$\begin{bmatrix} ACE_{G_i} = \sigma_{G_i} ACE_i \\ ACE_{B_i} = \sigma_{B_i} ACE_i \end{bmatrix}, \tag{7}$$

where σ_{B_i} and σ_{G_i} are allocation coefficients that represent the contributions of the BESS aggregator and the thermal power plant to load frequency control (LFC). Their sum is 1: $\sigma_{B_i} + \sigma_{G_i} = 1$. Assume that $\tau_b(t)$ is the time delay caused by the communication network when transmitting the control signal from the BESS aggregator to the b^{th} BESS. To ensure safety during charging and discharging, the power must be limited to the rated charging and discharging levels $\Delta P_B \in [P^{ch}_{r_{i,b}}, P^{dis}_{r_{i,b}}]$. Additionally, SoC of the BESS should remain within an upper and lower limit to prolong battery life, ranging from $SoC_{i,b} \in [SoC_{i,b_{\min}}, SoC_{i,b_{\max}}]$, namely 10 % and 90 %. The BESS should charge or discharge according to the provided ACE_{B_i}. If the ACE_{B_i} falls below the lower limit, the BESS needs to supply power. If it exceeds the upper limit, the BESS needs to absorb power.

B. Distributed BESS Frequency Control Method Based on Two-Layer MPCs

Figure 2 shows a block diagram of the distributed BESS frequency control method based on two-layer MPCs.

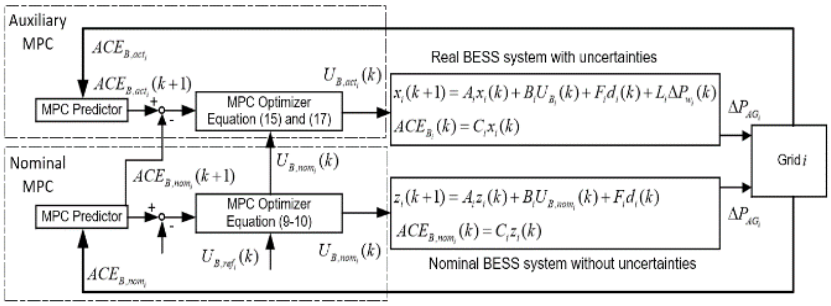

Fig. 2. Block diagram of distributed BESS frequency control based on double layer MPCs.

From Fig. 2, it can be seen that this paper uses a two-layer MPC approach to generate frequency control signals for the BESS. The approach achieves load frequency control (LFC) while optimising the cost function. Related constraints of BESS and the power system are considered to optimise the cost function [22]. The proposed two-layer MPC controller includes a nominal controller and an auxiliary controller. The state-space model of a system without uncertainties is assumed to be

$$\begin{cases} z_i(k+1) = A_i z_i(k) + B_i U_{B,nom_i}(k) + F_i d_i(k), \\ ACE_{B,nom_i}(k) = C_i z_i(k). \end{cases} \tag{8}$$

In the equation, $z(k)$ and $U_{B,nom_i}(k)$, respectively, represent the nominal system's state variables and control signals extracted from a nominal BESS system model without uncertainty. The control objective is to minimise the following objective function

$$\min_{U_{B,nom}} \sum_{k=0}^{p} Q_{ACE_{i,1}} (ACE_{B,nom_i}(k+1) - ACE_{B,ref_i}(k+1))^2 + \\ + \sum_{k=0}^{p} Q_{U_{B_{i,1}}} (\Delta U_{B,nom_i}(k))^2, \tag{9}$$

where $Q_{ACE_{i,1}}$ and $Q_{U_{B_{i,1}}}$, respectively, represent the weighting factors for nominal MPC inputs and outputs. Control signals, outputs, charging/discharging power, and SoC are constrained within a subset of the original constraints

$$\begin{bmatrix} \alpha ACE_{B_{i\min}} \le ACE_{B,nom_i} \le \alpha ACE_{B_{i\max}} \\ \alpha U_{B_{i\min}} \le U_{B,nom_i} \le \alpha U_{B_{i\max}} \\ \alpha P^{ch}_{r_{i,b}} \le P_{B,nom_{i,b}} \le \alpha P^{dis}_{r_{i,b}} \\ \frac{1}{1-\alpha} SoC_{i,b_{\min}} \le SoC_{nom_i,b} \le \alpha SoC_{i,b_{\max}} \end{bmatrix}, \tag{10}$$

where α represents the tuning coefficient, which takes values in the interval (0, 1). The above constraints are tightened constraints. The upper and lower bounds of the tightened constraints are part of the original constraints. In addition, auxiliary MPC aims at controlling systems with uncertainties. In auxiliary MPC, U_{B_i} and ACE_{B,nom_i} are obtained from the nominal controller, while ACE_{B,act_i} is obtained from the actual uncertain system. The discrete-time state-space model of the actual BESS system with uncertainties is

$$\begin{cases} x_i(k+1) = A_i x_i(k) + B_i U_{B_i}(k) + F_i d_i(k) + L_i \Delta P_{w_i}(k), \\ ACE_{B_i}(k) = C_i x_i(k), \end{cases} \tag{11}$$

where $x_i = [\Delta f_i, \Delta P_{tie}, \Delta P_{B_i,1} ... \Delta P_{B_i,N_{B_i}}]^{\mathrm{T}}$ represents the vector of state variables. The state matrix A_i and the input matrix B_i are, respectively,

$$A_i = \begin{bmatrix} \frac{-D_i}{2H_i} & \frac{-1}{2H_i} & \frac{1}{2H_i} & \cdots & \frac{1}{2H_i} \\ 2\pi \sum_{j \in M-\{i\}} T_{ij} & 0 & 0 & \cdots & 0 \\ 0 & 0 & \frac{-1}{T_{B_{N_1,i}}} & \cdots & 0 \\ \vdots & \vdots & \vdots & \ddots & \vdots \\ 0 & 0 & 0 & \cdots & \frac{-1}{T_{B_{N_B,i}}} \end{bmatrix}, \tag{12}$$

$$B_i = \begin{bmatrix} 0 & 0 & K_{B_{i,1}} & ... & K_{B_{i,N_{B_i}}} \end{bmatrix}^T, \tag{13}$$

and we can also make the assumption that the system input is $d_i = [\Delta P_{L_i}, \Delta P_{AR_i}, \Delta P_{m_i}]^{\mathrm{T}}$, where $\Delta P_{AR_i} = \sum_{j \in M-\{i\}} T_{ij}(\Delta f_i)$, L_i, F_i, and C_i can be denoted by:

$$L_i = \begin{bmatrix} \frac{1}{2H_i} & 0 & 0 & \ldots & 0 \end{bmatrix}^T, \tag{14}$$

$$F_i = \begin{bmatrix} \frac{-1}{2H_i} & 0 & \frac{1}{2H_i} \\ 0 & -2\pi & 0 \\ 0 & 0 & 0 \\ \vdots & \vdots & \vdots \\ 0 & 0 & 0 \end{bmatrix}, \tag{15}$$

$$C_i = \begin{bmatrix} \sigma_{B_i}\beta_i & \sigma_{B_i} & 0 & \ldots & 0 \end{bmatrix}^T. \tag{16}$$

This paper incorporates the uncertain output of wind power into the state-space equation as an additional disturbance. The MPC utilises the measured value of ACE_{B_i}, and then provides a control signal U_{B_i} to the system model, aiming to minimise the control effort while making the system output ACE_{B_i} as close as possible to the reference output ACE_{B,ref_i}, which is set to zero. The ultimate goal is to minimise the following objective function:

$$\min_{U_B} \sum_{k=0}^{p} Q_{ACE_i} (ACE_{B_i}(k+1) - ACE_{B,ref_i})^2 + \\ + \sum_{k=0}^{p} Q_{U_{B_i}} (\Delta U_{B_i}(k))^2, \tag{17}$$

$$\begin{bmatrix} ACE_{B_{i\min}} \le ACE_{B_i} \le ACE_{B_{i\max}} \\ U_{B_{i\min}} \le U_{B_{i\max}} \le U_{B_{i\max}} \\ P_{r,b}^{ch} \le P_{B_{i,b}} \le P_{r_{i,b}}^{dis} \\ SoC_{i,b_{\min}} \le SoC_{i,b} \le SoC_{i,b_{\max}} \end{bmatrix}, \tag{18}$$

where Q_{ACE_i} and $Q_{U_{B_i}}$, respectively, represent the weighting factors for MPC input and output, p and c represent the prediction layer and control layer, respectively, $ACE_{B_{i\min}}$, $ACE_{B_{i\max}}$, $U_{B_{i\min}}$, and $U_{B_{i\max}}$ represent the constraints imposed on the minimum and maximum values of ACE and MPC output within the prediction and control ranges. ACE_{B,act_i} can be represented as

$$ACE_{B,\mathrm{act}_i}(k) = C_i x_i(k). \tag{19}$$

The auxiliary controller generates the control signal $U_{B,act}$ to minimise the following objective function

$$\min_{U_{B,act}} \sum_{k=0}^{p} Q_{ACE_{i,2}} \left(ACE_{B,act_i}(k+1) - ACE_{B_i,nom_i}(k+1) \right)^2 + \\ + \sum_{k=0}^{c} Q_{U_{B_{i,2}}} \left(U_{B,act_i}(k) - U_{B,nom_i}(k) \right)^2, \tag{20}$$

where $Q_{ACE_{i,2}}$ and $\sum_{k=0}^{c} Q_{U_{B_{i,2}}}$, respectively, represent the weighting factors associated with the inputs and outputs of the auxiliary MPC. The auxiliary MPC needs to generate a series of control signals Q_{ACE_i} to minimise the difference between the trajectory and control signals of the actual system and those of the nominal system. The first term sum in (20) represents the ACE error between the nominal and actual systems within the prediction horizon, while the second term sum in (20) represents the command signal generated relative to the nominal MPC error within the control range. The optimisation process in (20) is limited to the constraints in (18), which are referred to as the original constraints. As represented, respectively, in (10) and (18), the original and tightening constraints, the auxiliary controller generates a trajectory within the pipe for the uncertain system (i.e., the nominal system), centred around an uncertainty-free system. The size of the pipe that the auxiliary MPC trajectory must preserve depends on the distance between the nominal system trajectory and the original boundaries. The two-layer MPC controller generates a control sequence to minimise the deviation between the trajectories of the actual system and the

nominal system. In practical uncertain systems, when the BESS synthesis control is performed in this order, the trajectory of the uncertain system approaches the nominal trajectory generated by the nominal MPC. Therefore, the weighting factors of the nominal and auxiliary MPCs are adjusted simultaneously by minimising the following objective function:

$$\min \sum_{i\in M}\int_0^{T_f} t(\Delta f_i(t)^2)dt + \sum_{\substack{i\in M\\ j\in M\\ j\neq i}}\int_0^{T_p} t(\Delta P_{tie_{i-j}}(t)^2)dt, \quad (21)$$

$$\left[\begin{array}{l} Q_{ACE_{i,r_{\min}}} \le Q_{ACE_{i,r}} \le Q_{ACE_{i,r_{\max}}} \\ Q_{U_{B_{i,r_{\min}}}} \le Q_{U_{B_{i,r}}} \le Q_{U_{B_{i,r_{\max}}}} \end{array}\right]. \quad (22)$$

In (21), $\Delta f_i(t)$ represents the frequency deviation in the control area, and $\Delta P_{tie}(t)$ represents the tie-line power deviation. T_f and T_p are the time lengths for frequency and tie-line deviations, respectively. The subscripts $r_{1,2}$ denote the nominal and auxiliary MPCs, respectively. As shown in (21), the time integration multiplied by the square error is used to obtain the optimal solution. In this paper, the sine cosine algorithm (SCA) is utilised to implement these solutions.

C. Coordinated Controller for Thermal Power Plants and BESS Based on Fuzzy Inference System

During communication delays, thermal power plants compensate for the system's active power imbalance by either increasing or decreasing their output power from the grid. However, if BESS provides command output or absorbs additional power based on long-term delays, serious frequency violations may occur in the grid. Therefore, this paper adopts a fuzzy logic controller to adjust the operation of thermal generators using adjustment signals associated with the BESS aggregator. The fuzzy inference system is an intelligent control method based on fuzzy set theory, fuzzy linguistic variables, and fuzzy logic reasoning, which mimics human fuzzy reasoning and decision-making processes behaviourally. In this control method, expert experience or operator actions are first encoded into fuzzy rules, and then real-time signals from sensors are fuzzified. The fuzzified signals serve as inputs to the fuzzy rules, completing fuzzy inference, and the inferred output quantities are added to the actuators.

In Fig. 3, ΔP_{AG_i} and ACE_{G_i} represent the output power of the BESS aggregator and the thermal power plant, respectively, k_1, k_2, and k_3 are fuzzification coefficients, while k_4 and k_5 are the defuzzification coefficient; k_p and k_i are the gain coefficients of the proportional-integral (PI) controller. In this paper, a PI controller is used to generate control signals to adjust the output power of the thermal power plant. As shown in the figure, the input variables of this fuzzy controller are the output power of the BESS aggregator ΔP_{AG_i} and the output power of the thermal power plant ACE_{G_i}. The output is the output power of the thermal power plant. The working principle of the proposed fuzzy coordinator is as follows. First, fuzzification is performed. The input of the fuzzy controller must be fuzzified before they can be used to solve the output, so the real deterministic input must be transformed into a fuzzy vector. In this paper, the input variables, including the output power of the BESS aggregator ΔP_{AG_i} and the output power of the thermal power plant ACE_{G_i}, and their rate of change, must be converted to fuzzy quantities.

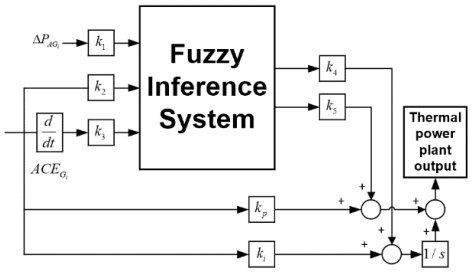

Fig. 3. Proposed coordination scheme between the BESS aggregator and the CPP.

From Fig. 4, it can be observed that the membership functions corresponding to the controller inputs are negative (N), zero (Z), and positive (P), while the membership functions for the output variables are arranged as large negative (LN), small negative (SN), zero (ZR), small positive (SP), and large positive (LP). Each membership function defines its own weight and provides linguistic variables. Then, the linguistically variables after fuzzification enter the fuzzy inference system. The rule base defined in the fuzzy inference system can provide inference results. For example, when the output power and its rate of change of the thermal power plant are negative (N) and the output power of the BESS aggregator is negative (N), the fuzzy output is obtained as negative (N).

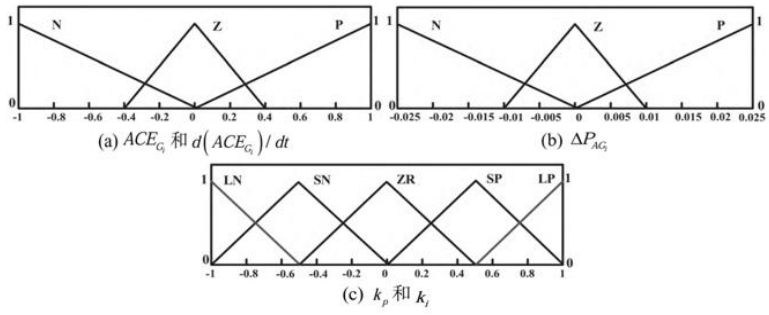

(a) ACE_{G_i} 和 $d\left(ACE_{G_i}\right)/dt$ (b) ΔP_{AG_i}

(c) k_p 和 k_i

Fig. 4. Membership functions for inputs and outputs.

This paper employs a set of 27 fuzzy rules, and the proposed fuzzy controller aims to perform online adjustments

to the gains of the PI controller. Finally, the linguistic variables are defuzzified and after applying the defuzzification coefficient, the adjustment signal is provided to the thermal power plant.

III. SIMULATION ANALYSIS AND VERIFICATION

To verify the effectiveness and superiority of the proposed method, a simulation analysis was conducted on the IEEE 39-bus test system. Figure 5 shows the schematic diagram of the improved IEEE 39-bus test system. This test system includes 10 generators (G1–G10) and three wind farms (WT1–WT3) with a total generation capacity of 60 MW, located in buses 5, 26, and 16 in areas 1, 2, and 3, respectively. Each wind farm has an average generation power of 20 MW. Figure 6 shows the wind speed fluctuations for the three areas. Areas 1 and 2 have two battery energy storage system (BESS) aggregators (with capacities of 4.68 MWh and 5.25 MWh, respectively), each controlling five distributed BESS units. Table I provides the relevant parameters of the BESS units distributed [10]. Table II shows the weight coefficient after optimisation. The rated charging and discharging power of a single BESS is 500 kW. It is assumed that the area control error (ACE) is allocated to conventional power plant (CPP) and BESS with distribution coefficients of 0.6 and 0.4, respectively. The dead-band upper and lower limits for the ACE_B area are 0.01 p.u. The control and prediction horizons of the dual-layer MPC are 2 and 20, respectively, with a sampling interval of 0.1 seconds. The constraints of the nominal MPC are tightened to 80 % of the auxiliary MPC constraints.

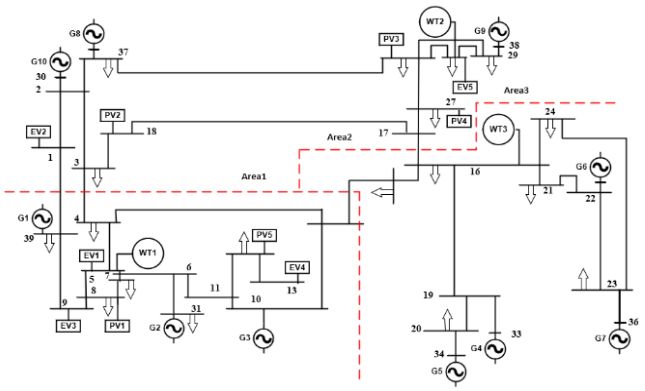

Fig. 5. Single line diagram of IEEE 39 node test system.

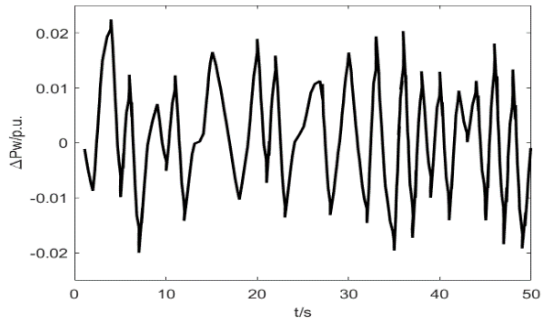

Fig. 6. Fluctuation in wind power.

To provide a better quantitative factor that exposes how much better the proposed method is compared to the others, you could use a performance improvement index (PII) calculated as follows

$$PII = \left(\frac{TraMPC\ Metric - ProMPC\ Metric}{TraMPC\ Metric} \right) \times 100\%. \quad (23)$$

The proposed dual-layer MPC demonstrates significant improvements in response time, frequency deviation, and tie-line power deviation. These improvements are quantified using the performance improvement index (*PII*).

TABLE I. PARAMETERS OF DISTRIBUTED BESS.

Area	BESS	K_B^{ch}, K_B^{dis}	T_B	Initial *SoC*	Cap. MWh
1	1	25	0.5	60 %	1
	2	22.5	0.4	60 %	0.88
	3	24.5	0.9	58 %	0.81
	4	28	0.7	50 %	0.99
	5	27	0.8	70 %	0.96
2	1	23.75	0.2	62 %	0.93
	2	30	0.6	49 %	1.16
	3	28.75	0.5	53 %	1.17
	4	21.25	0.7	68 %	0.99
	5	20	0.3	75 %	0.96

TABLE II. WEIGHTING COEFFICIENTS IN MPCS OBJECTIVE FUNCTION.

Method	$Q_{ACE1.1}$	$Q_{U1.1}$	$Q_{ACE1.2}$	$Q_{U1.2}$
Dual-layer MPC	0.7065	0.8441	1.0025	0.6937
	$Q_{ACE2.1}$	$Q_{U2.1}$	$Q_{ACE2.2}$	$Q_{U2.2}$
Dual-layer MPC	0.5008	1.1170	0.8320	0.4322
	Q_{ACE1}	Q_{UB1}	Q_{ACE2}	Q_{UB2}
Single-layer MPC	1.2036	0.6312	0.7955	0.4637

Dynamic Performance Verification. To verify the dynamic performance of the proposed controller, this paper assumes a load increase of 10 MW in Area 1 at t = 10 s and a load decrease of 10 MW in Area 2 at t = 30 s. Figures 7 and 8 show the deviation in frequency and tie-line power of the test system. The simulation results include the dynamic responses related to traditional MPC, nominal MPC, and auxiliary MPC. The results of the nominal MPC are related to the case without uncertainties. The simulation results indicate that, compared to traditional MPCs, the proposed dual-layer controller significantly reduces deviations, and, in the absence of uncertainties, the trajectory of the proposed controller remains very close to that of the nominal MPC.

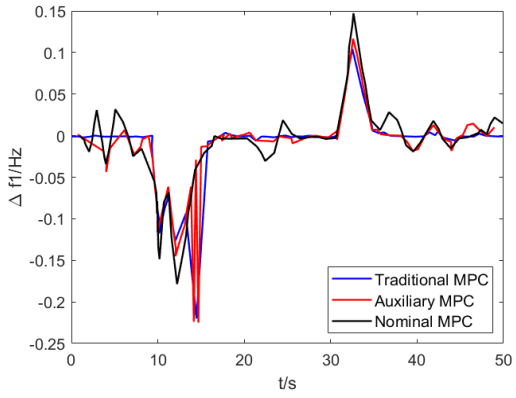

Fig. 7. Comparison between the proposed controller and conventional MPC (Δf_1).

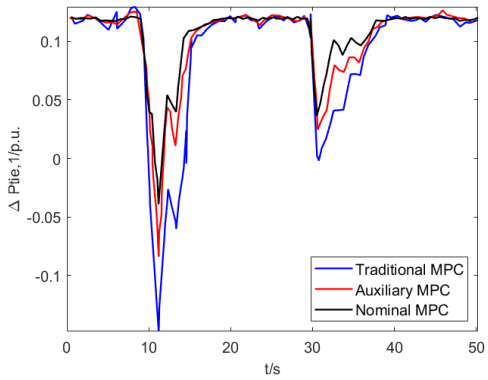

Fig. 8. Comparison between the proposed controller and conventional MPC $(\Delta P_{tie,1})$.

Figures 9 and 10 show the output power of the two aggregators under the proposed MPC and the traditional MPC.

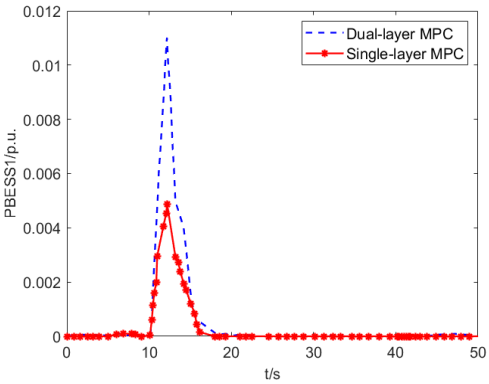

Fig. 9. Output power of BESS aggregators in areas (Area 1).

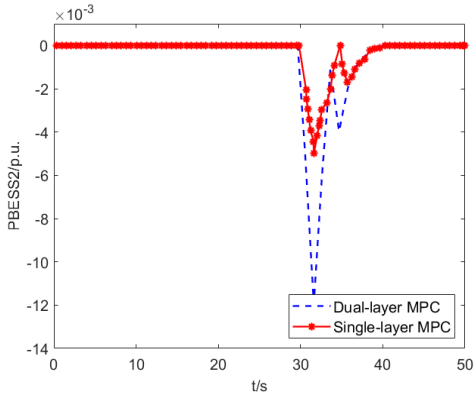

Fig. 10. Output power of BESS aggregators in areas (Area 2).

As shown in Figs. 9 and 10, the BESS aggregators with the proposed controller respond faster within the rated power limits and can maintain area frequency stability. Additionally, the BESS aggregators under the proposed controller can provide more power and energy to the system. Figure 11 shows the output power of each BESS under the proposed dual-layer controller. From Fig. 11, it can be seen that the first five BESS units in Area 1 respond to the load changes in Area 1, while their response to load changes in Area 2 is minimal. Conversely, the BESS units in Area 2 show a greater response to the load changes in Area 2, indicating that BESS units with higher charge/discharge coefficients and lower time constants contribute more significantly to load frequency control (LFC). Taking BESS 9 in Area 2 as an example, it has the highest time constant and relatively lower charge/discharge coefficients, making thus the smallest contribution among the BESS units in Area 2.

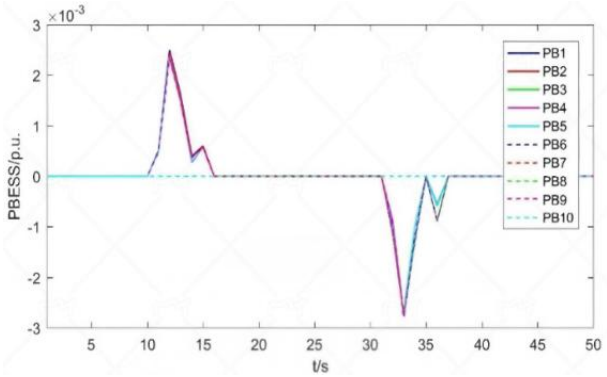

Fig. 11. The output power of individual BESSs.

This paper assumes that the power sum of the tie lines connected to Area i equals $P_{\text{tie},i}$. Therefore, changes in tie-line power are represented as additive disturbances in the state-space equation. Uncertainty in the tie-line power flow between Areas 1 and 2 is assumed to verify the performance of the proposed controller in handling uncertainties. This uncertainty is modelled as a uniform disturbance with upper and lower bounds at 2 % of the absolute value of the actual value. It is assumed that at t = 10 s, the load in Area 1 increases by 10 MW. Figures 12 and 13 show the deviations in area frequency and tie-line power under uncertainties in wind turbine power and tie-line power. The simulation results validate the superiority of the proposed controller in dealing with uncertainties.

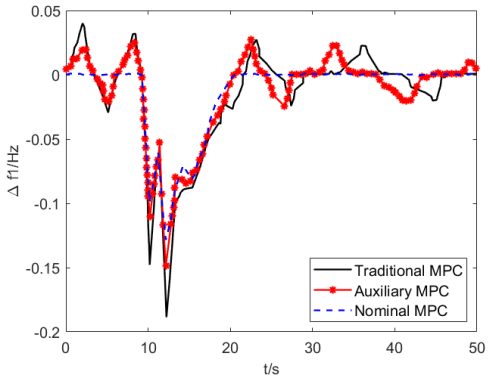

Fig. 12. Performance of the proposed controller for uncertainty in tie-line power and wind generation (Δf_1).

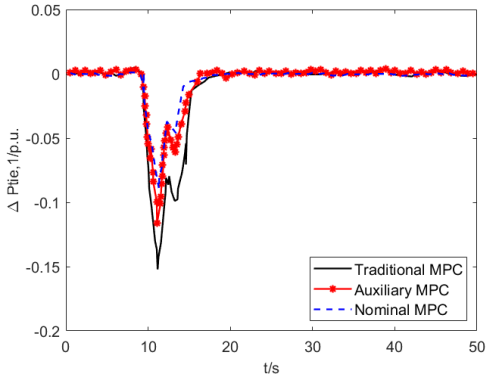

Fig. 13. Outlier identification outcome.

IV. CONCLUSIONS

This paper proposes a dual-layer model predictive control (MPC) method to control distributed battery energy storage system (BESS) aggregators in a smart grid to enhance load frequency control performance. The proposed MPC controller can handle system constraints and BESS constraints. The simulation results show that, compared to traditional MPC, the dual-layer MPC has certain advantages in reducing frequency deviations, tie-line power deviations, and handling uncertainties. Additionally, the proposed control method enables distributed BESS to provide and withdraw higher levels of power and respond faster, ensuring better frequency regulation. Compared to scenarios without coordination and with traditional MPC, the intelligent coordination scheme results in smaller frequency and tie-line power deviations. The ability of the dual-layer MPC to manage both the nominal and auxiliary control layers allows it to effectively address uncertainties in the power system, which is crucial given the increasing penetration of renewable energy sources that introduce variability and unpredictability into the grid. The results indicate that, compared to scenarios without coordination and with traditional MPC, the intelligent coordination scheme results in smaller frequency and tie-line power deviations. In the future, this paper will explore the coordination among different types of energy storage systems to achieve frequency regulation.

CONFLICTS OF INTEREST

The authors declare that they have no conflicts of interest.

REFERENCES

[1] T. Ngoc-Hung, "Optimising damping control in renewable energy systems through reinforcement learning within wide-area measurement frameworks", *Elektronika ir Elektrotechnika*, vol. 30, no. 3, pp. 32–45, 2024. DOI: 10.5755/j02.eie.36385.

[2] V. Sinik, Z. Despotovic, and I. Palinkas, "Optimization of the operation and frequency control of electromagnetic vibratory feeders", *Elektronika ir Elektrotechnika*, vol. 22, no. 1, pp. 24–30, 2016. DOI: 10.5755/j01.eee.22.1.14095.

[3] Z. Civelek, G. Gorel, M. Luy, N. Barısci, and E. Cam, "Effects on load-frequency control of a solar power system with a two-area interconnected thermal power plant and its control with a new BFA algorithm", *Elektronika ir Elektrotechnika*, vol. 24, no. 6, pp. 3–10, 2018. DOI: 10.5755/j01.eie.24.6.22281.

[4] H. Zhao, Q. Wu, C. Wang, L. Cheng, and C. N. Rasmussen, "Fuzzy logic based coordinated control of battery energy storage system and dispatchable distributed generation for microgrid", *Journal of Modern Power Systems and Clean Energy*, vol. 3, no. 3, pp. 422–428, 2015. DOI: 10.1007/s40565-015-0119-x.

[5] A. Urtasun, E. L. Barrios, P. Sanchis, and L. Marroyo, "Frequency based energy management strategy for stand-alone systems with distributed battery storage", *IEEE Transactions on Power Electronics*, vol. 30, no. 9, pp. 4794–4808, 2015. DOI: 10.1109/TPEL.2014.2364861.

[6] P. Mercier, R. Cherkaoui, and A. Oudalov, "Optimizing a battery energy storage system for frequency control application in an isolated power system", *IEEE Transactions on Power Systems*, vol. 24, no. 3, pp. 1469–1477, 2009. DOI: 10.1109/TPWRS.2009.2022977.

[7] S. Sitompul and G. Fujita, "Impact of state-of-charge control integrated with load-frequency control on battery energy storage system in islanded microgrid system", in *Proc. of 2021 IEEE 12th Energy Conversion Congress & Exposition - Asia (ECCE-Asia)*, 2021, pp. 199–203. DOI: 10.1109/ECCE-Asia49820.2021.9479179.

[8] D.-I. Stroe, V. Knap, M. Swierczynski, A.-I. Stroe, and R. Teodorescu, "Operation of a grid-connected Lithium-ion battery energy storage system for primary frequency regulation: A battery lifetime perspective", *IEEE Transactions on Industry Applications*, vol. 53, no. 1, pp. 430–438, 2017. DOI: 10.1109/TIA.2016.2616319.

[9] L. Xing *et al.*, "Dual-consensus-based distributed frequency control for multiple energy storage systems", *IEEE Transactions on Smart Grid*, vol. 10, no. 6, pp. 6396–6403, 2019. DOI: 10.1109/TSG.2019.2904075.

[10] T. Zhao, A. Parisio, and J. V. Milanović, "Distributed control of battery energy storage systems for improved frequency regulation", *IEEE Transactions on Power Systems*, vol. 35, no. 5, pp. 3729–3738, 2020. DOI: 10.1109/TPWRS.2020.2974026.

[11] S.-J. Lee *et al.*, "Coordinated control algorithm for distributed battery energy storage systems for mitigating voltage and frequency deviations", *IEEE Transactions on Smart Grid*, vol. 7, no. 3, pp. 1713–1722, 2016. DOI: 10.1109/TSG.2015.2429919.

[12] Y. J. A. Zhang, C. Zhao, W. Tang, and S. H. Low, "Profit-maximizing planning and control of battery energy storage systems for primary frequency control", *IEEE Transactions on Smart Grid*, vol. 9, no. 2, pp. 712–723, 2018. DOI: 10.1109/TSG.2016.2562672.

[13] J. W. Shim, G. Verbič, K. An, J. H. Lee, and K. Hur, "Decentralized operation of multiple energy storage systems: SOC management for frequency regulation", in *Proc. of 2016 IEEE International Conference on Power System Technology (POWERCON)*, 2016, pp. 1–5. DOI: 10.1109/POWERCON.2016.7754038.

[14] D. Zhu and Y.-J. A. Zhang, "Optimal coordinated control of multiple battery energy storage systems for primary frequency regulation", *IEEE Transactions on Power Systems*, vol. 34, no. 1, pp. 555–565, 2019. DOI: 10.1109/TPWRS.2018.2868504.

[15] A. S. Musleh, S. M. Muyeen, A. Al-Durra, I. Kamwa, M. A. S. Masoum, and S. Islam, "Time-delay analysis of wide-area voltage control considering smart grid contingences in a real-time environment", *IEEE Transactions on Industrial Informatics*, vol. 14, no. 3, pp. 1242–1252, 2018. DOI: 10.1109/TII.2018.2799594.

[16] X. Liu, Y. Zhang, and K. Y. Lee, "Coordinated distributed MPC for load frequency control of power system with wind farms", *IEEE Transactions on Industrial Electronics*, vol. 64, no. 6, pp. 5140–5150, 2017. DOI: 10.1109/TIE.2016.2642882.

[17] X. Sun, K. Liao, J. Yang, and Z. He, "Model predictive control based load frequency control for power systems with wind turbine generators", in *Proc. of 2019 IEEE Innovative Smart Grid Technologies - Asia (ISGT Asia)*, 2019, pp. 1387–1392. DOI: 10.1109/ISGT-Asia.2019.8881147.

[18] X. Liu, X. Kong, and K. Y. Lee, "Distributed model predictive control for load frequency control with dynamic fuzzy valve position modelling for hydro–thermal power system", *IET Control Theory Applications*, vol. 10, no. 14, pp. 1653–1664, 2016. DOI: 10.1049/iet-cta.2015.1021.

[19] F. Yang, S. Yu, J. Zhao, D. Li, and S. Lin, "Distributed reconfigurable model predictive control based load frequency control of microgrid clusters with dynamic topology", *Electric Power Systems Research*, vol. 221, art. 109445, 2023. DOI: 10.1016/j.epsr.2023.109445.

[20] Y. Zheng, J. Zhou, Y. Xu, Y. Zhang, and Z. Qian, "A distributed model predictive control based load frequency control scheme for multi-area interconnected power system using discrete-time Laguerre functions", *ISA Transactions*, vol. 68, pp. 127–140, 2017. DOI: 10.1016/j.isatra.2017.03.009.

[21] Y. Xie, H. Li, and H. Cui, "Load restoration strategy for power system considering the transient frequency control ability of energy storage system", *Electric Power Engineering Technology*, vol. 40, no. 6, pp. 43–51, 2021. DOI: 10.12158/j.2096-3203.2021.06.006.

[22] S. Yan, W. Wang, and X. Li, "Cross-regional flexible robust optimal scheduling in dynamic economic environment with joint frequency regulation of energy storage and units", *Automation of Electric Power Systems*, vol. 46, no. 9, pp. 61–70, 2022. DOI: 10.7500/AEPS20210508002.